ACS APPLIED MATERIALS & INTERFACES

Research Article

www.acsami.org

Designed Fabrication of Unique Eccentric Mesoporous Silica Nanocluster-Based Core–Shell Nanostructures for pH-Responsive Drug Delivery

Lulu Chen,[†,⊥] Lu Li,[†,⊥] Lingyu Zhang,[†] Shuangxi Xing,[†] Tingting Wang,*[,‡] Y. Andrew Wang,[§] Chungang Wang,*[,†] and Zhongmin Su[†]

[†]Faculty of Chemistry, Northeast Normal University, Changchun, 130024 P.R. China

[‡]School of Chemistry & Environmental Engineering, Changchun University of Science and Technology, Changchun, 130022, P.R. China

[§]Ocean Nanotech, LLC, Springdale, Arkansas 72764, United States

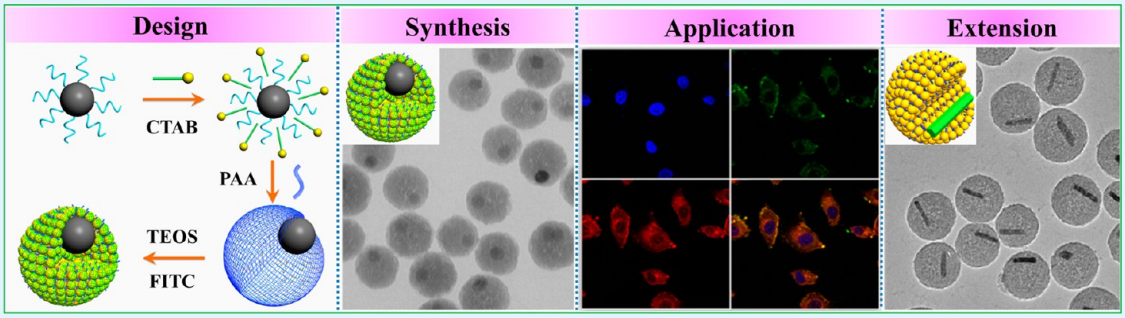

ABSTRACT: A novel and facile strategy using poly(acrylic acid) (PAA) as a nanoreactor and template has been proposed and applied for the first time to fabricate a novel and unique class of multifunctional eccentric Fe_3O_4@PAA/SiO_2 core–shell nanoclusters (NCs) consisting of a single Fe_3O_4 nanoparticle (NP), PAA, and eccentric SiO_2 NCs that are composed of a large number of small fluorescent SiO_2 NPs. Interestingly, the resulting eccentric PAA shell around Fe_3O_4 NPs as a high water-absorbent polymer is like a "reservoir" to absorb and retain water molecules inside its net structure to confine the growth of small SiO_2 NPs inside the PAA networks, resulting in the formation of an eccentric SiO_2 NC with aggregated pores. The thicknesses of uniform and well-dispersed SiO_2 NCs can also be precisely controlled by varying the amount of tetraethyl orthosilicate (TEOS). Importantly, the synthetic method has been confirmed to be universal and extended to other functional NPs with different compositions and shapes as eccentric cores. Furthermore, the as-prepared multifunctional eccentric Fe_3O_4@PAA/SiO_2 core–shell NCs combined fluorescence imaging, ultrahigh drug loading capacity (1.13 mg doxorubicin/mg eccentric NCs), and pH-responsive drug release into one were taken as an example to study the applications in simultaneous fluorescence imaging and pH responsive drug delivery into prostate cancer PC3M cells.

KEYWORDS: *eccentric core–shell structure, poly(acrylic acid) nanoreactor, mesoporous silica nanoclusters, fluorescence imaging, pH response*

INTRODUCTION

Multifunctional nanoparticles (NPs) based on mesoporous SiO_2 ($mSiO_2$) nanostructures have been developed as nanomedical platforms for multimodal imaging or simultaneous diagnosis and therapy.[1−7] Different functional components, such as magnetic,[8,9] up-conversion,[10,11] plasmonic NPs,[12,13] quantum dots,[14,15] and fluorescent dyes[16,17] have been encapsulated into $mSiO_2$ shells to obtain concentric multifunctional core–shell nanostructures, which can maintain their individual function when they are utilized as a nanocarrier for fluorescence imaging, magnetic resonance imaging (MRI), and delivering anticancer drugs and genes to the tumor tissues for cancer diagnostics and therapy.[3,18−31] Up to now, versatile concentric $mSiO_2$-based multifunctional core–shell NPs consisting of various functional NPs within $mSiO_2$ shell were generally fabricated using cetyltrimethylammonium bromide (CTAB) as pore-generating templates by sol–gel processing.[32−37] For example, Hyeon et al. presented discrete and monodisperse Fe_3O_4@$mSiO_2$ core–shell NPs for simultaneous MRI, fluorescence imaging, and drug delivery.[35] Shi et al. prepared up-conversion $NaYF_4$:Tm/Yb/Gd@$mSiO_2$ core–shell NPs for bioimaging.[10] Chen and co-workers reported the fabrication of gold nanorods (NRs)@$mSiO_2$ core–shell NPs as a theranostic platform for cancer treatment.[13] However, some tedious steps were involved to obtain the multifunctional

Received: May 1, 2013
Accepted: June 28, 2013
Published: June 28, 2013

concentric $mSiO_2$-based NPs, such as the removal of CTAB templates by using a solvent or calcinations.[37,38]

Recently, a pH-responsive delivery polymer system represents an effective strategy for cancer therapies, because NPs can be delivered to acidic tumor sites via the enhanced permeability and retention (EPR) effect. As a result, the internalized NPs are generally entrapped in acidic endosomes (pH 5.5−6.0).[39−41] To endow the multifunctional $mSiO_2$-based NPs with pH-responsive drug delivery capability, various pH-sensitive polymers were utilized to graft onto the surface of $mSiO_2$ to construct pH-responsive controlled drug delivery systems.[42−47] For instance, Hu et al. successfully modified poly(acrylic acid) (PAA) onto amino group functionalized $mSiO_2$ NPs through the amidation reaction, which were utilized as pH-responsive drug delivery carriers.[42] Che et al. reported the fabrication of a novel coordination polymer-coated $mSiO_2$ NP loading drug for pH-responsive drug delivery.[43] Yang and co-workers developed the pH-responsive composite microspheres, consisting of a concentric Fe_3O_4@$mSiO_2$ NP and a shell of cross-linked poly (methacrylic acid) (PMAA) by distillation precipitation polymerization.[44] Lin et al. demonstrated a controlled release system based on up-conversion luminescent microspheres of $NaYF_4$:Yb^{3+}/Er^{3+} coated with the pH-triggered thermally sensitive hydrogel poly[(*N*-isopropylacrylamide)-*co*-(methacrylic acid)] [P(NIPAM-*co*-MAA)] by aqueous phase radical polymerization.[45] However, problems were involved in the aforementioned system including low drug loading capacity and complicated preparation steps. As we know so far, there is no report on the fabrication of multifunctional eccentric NP-based $mSiO_2$ using a templating agent that not only acts as mesopore-generating templates but also serves as a pH-responsive controlled drug delivery system without complex surface modification and postprocessing steps.

Herein, we first develop a facile and novel method to prepare a new and unique class of multifunctional eccentric Fe_3O_4@PAA/SiO_2 core−shell nanoclusters (NCs) consisting of a single Fe_3O_4 NP, PAA, and SiO_2 NCs that are composed of a large number of small fluorescent SiO_2 NPs using PAA as a nanoreactor and template. Moreover, the thicknesses of SiO_2 NCs can also be precisely controlled. Importantly, the synthetic strategy is universal and has been extended to other functional NPs with different compositions and shapes as eccentric cores. In our method, constructing an eccentric $mSiO_2$ NC on PAA template and encapsulating PAA chains for drug loading in the shell are integrated in one step, which can endow multifunctional NP-based $mSiO_2$ core−shell nanostructures with an effective pH-responsive drug delivery ability. Therefore, to illustrate the as-prepared multifunctional eccentric NCs for the potential applications in nanomedicine, the fluorescent−magnetic eccentric Fe_3O_4@PAA/SiO_2 core−shell NCs were taken as an example to study the applications in simultaneous fluorescence imaging and pH-responsive drug delivery into cancer cells.

EXPERIMENTAL SECTION

Chemicals. Oleylamine (OMA) and oleic acid (OA) modified superparamagnetic iron oxide NPs (Fe_3O_4 NPs) were obtained from Ocean Nano Tech. Cetyltrimethylammonium bromide (CTAB, ≥99%), fluorescein isothiocyanate (FITC), tetraethyl orthosilicate (TEOS, ≥98%), poly(acrylic acid) (PAA, $M_w \approx 1800$), and doxorubicin hydrochloride (DOX) were purchased from Sigma (USA). Isopropyl alcohol, ammonia solution (25−28%), gadolinium chloride hexahydrate ($GdCl_3{\cdot}6H_2O$), ytterbium chloride hexahydrate ($YbCl_3{\cdot}6H_2O$), erbium chloride hexahydrate ($ErCl_3{\cdot}6H_2O$), OA, and ammonium fluoride (NH_4F) were purchased from Sinopharm Chemical Reagent Beijing Co., Ltd. Deionized water was used in all experiments.

Characterization. Transmission electron microscopy (TEM) was measured on a JEOL-2100F transmission electron microscope under 200 kV accelerating voltage. Scanning electron microscopy (SEM) was performed on an XL30 ESEM-FEG field-emission scanning electron microscope (FEI Co.). Particle size distribution was obtained using a Mastersizer 2000 laser particle size analyzer. An up-conversion luminescence spectrum was measured using a RF5310 fluorescence spectrometer with an external 0−1 W adjustable CW laser at 980 nm as the excitation source. Thermogravimetric analysis (TG) was acquired from a Perkin-Elmer TG-7 analyzer heated from room temperature to 1000 °C at a ramp rate of 10 °C/min in air. Fluorescence spectra were carried out by an Eclipse fluorescence spectrophotometer (Varian, USA). Fourier transform infrared (FTIR) spectra were acquired by a Magna560 FTIR spectrometer (Nicolet, USA). The magnetic measurement was measured on a superconducting quantum interference device magnetometer (SQUIDMPMS XL-7) with fields up to 1.5 T. X-ray powder diffraction (XRD) patterns were performed on a D8 Focus diffractometer (Bruker) with Cu Kα radiation. N_2 adsorption/desorption measurements were performed by an intelligent gravimetric analyzer Autosorb-iQ (Quantachrome). UV−vis absorption spectroscopy was operated on a U-3010 spectro-photometer (Hitachi, Japan). Confocal laser scanning microscopy (CLSM) was obtained on an Olympus Fluoview FV1000.

Synthesis of CTAB Modification of Fe_3O_4 NPs. Monodisperse CTAB modified Fe_3O_4 NPs were prepared according to the previous report.[35] First, 500 μL of approximately 25 nm Fe_3O_4 NPs (10 mg mL^{-1}) capped with OA were added into 10 mL of CTAB aqueous solution (0.2 mol mL^{-1}) under magnetic stirring at 32 °C. After 30 min, the temperature was increased to 60 °C for another 20 min to volatilize OA, followed by cooling to room temperature. Finally, CTAB modified Fe_3O_4 NPs were collected by centrifugation and redispersed in 5 mL of deionized water.

Synthesis of Eccentric Fe_3O_4@PAA Core−Shell NPs. The method of the PAA coating onto Fe_3O_4 NPs was developed by our previously published work.[48] Typically, 40 μL of PAA aqueous solution (0.2 g mL^{-1}) and 60 μL of $NH_3{\cdot}H_2O$ (2 mol L^{-1}) were subsequently added into 5 mL of CTAB modified Fe_3O_4 NPs aqueous solution in a flask (250 mL), and the suspension was ultrasonicated for 30 min to disperse Fe_3O_4 NPs into solution. Then, 120 mL of isopropyl alcohol were added drop by drop into the mixture under magnetic stirring to obtain eccentric Fe_3O_4@PAA core−shell NPs.

Synthesis of FITC-Labeled Eccentric Fe_3O_4@PAA/SiO_2 Core−Shell NCs. To incorporate fluorescein isothiocyanate (FITC) into SiO_2 shell, 4 mg of FITC was covalently linked to 44 μL of 3-aminopropytrimethoxysilane (APTMS) in 1 mL of isopropyl alcohol overnight under dark condition for further use.[49] After adjusting the pH value of 15 mL of as-obtained eccentric Fe_3O_4@PAA core−shell NP solution to ∼8 with $NH_3{\cdot}H_2O$ solution (2 mol L^{-1}), 5 μL of the FITC-APTMS isopropyl alcohol solution was added into the mixture. Then, the addition of 500 μL of TEOS (20% in isopropyl alcohol) was carried out ten times for every 30 min intervals. After stirring for 24 h, the resulting FITC-labeled eccentric Fe_3O_4@PAA/SiO_2 core−shell NCs were collected by centrifugation and washed with isopropyl alcohol repeatedly so that the excess precursors were removed.

Synthesis of Eccentric $NaYF_4$:Yb/Er/Gd@PAA/SiO_2 Core−Shell NCs. Uniform and monodisperse OA capped $NaYF_4$:Yb/Er/Gd NRs were fabricated using the previously reported method.[50] Typically, 500 μL of the oleic acid stabilized $NaYF_4$:Yb/Er/Gd NRs in cyclohexane was mixed with 10 mL of CTAB aqueous solution (0.2 mol mL^{-1}) under vigorous magnetic stirring, and the suspension was heated to 80 °C to volatilize cyclohexane for 30 min. After being centrifuged, the NRs were redispersed in 5 mL of deionized water. According to the synthetic steps of eccentric Fe_3O_4@PAA/SiO_2 core−shell NCs, we could get eccentric $NaYF_4$:Yb/Er/Gd@PAA/SiO_2 core−shell NCs.

Scheme 1. Schematic Illustration of the Synthetic Procedure for the Eccentric Fe_3O_4@PAA/SiO_2 Core–Shell NCs and Application for pH-Dependent Drug Release and Fluorescence Imaging after Endocytosis in Prostate Cancer PC3M Cells

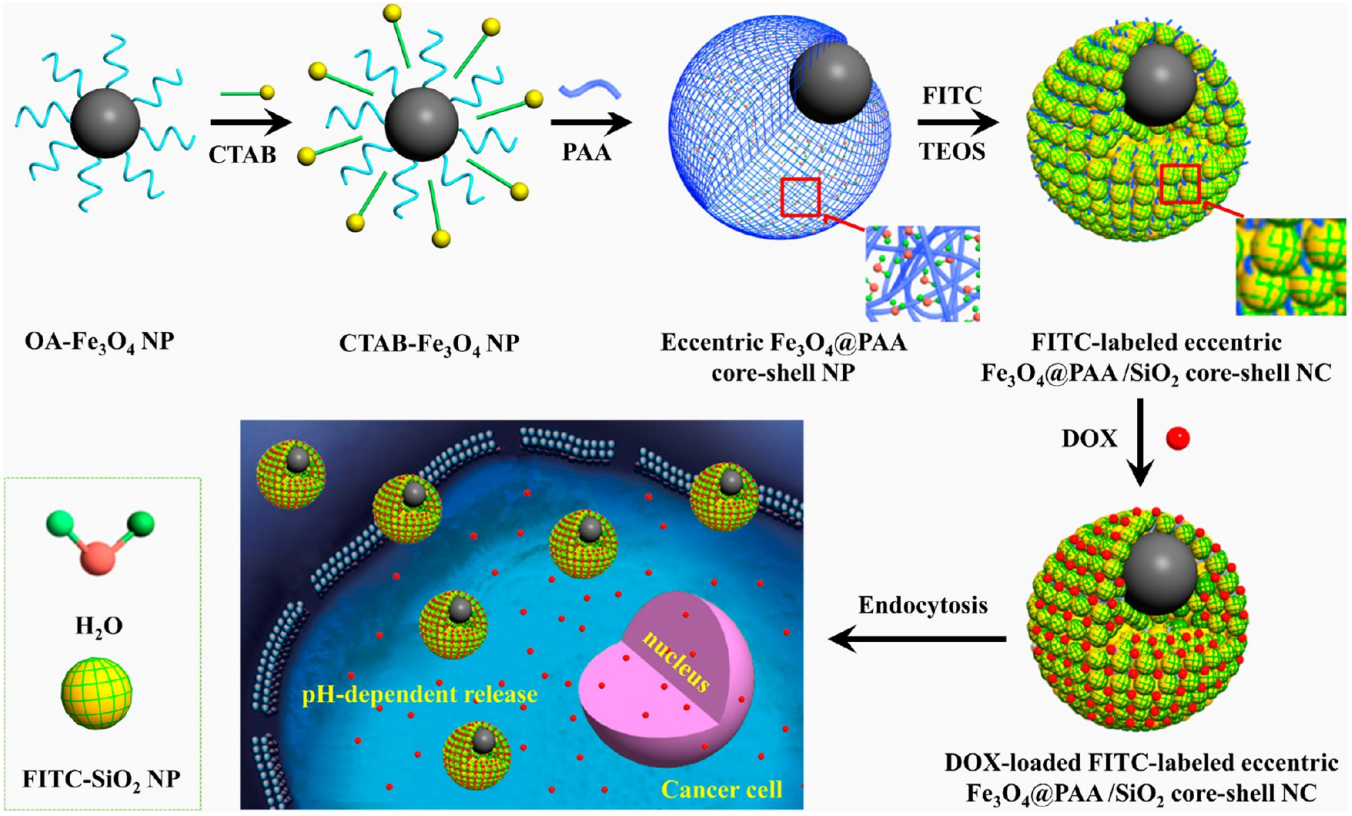

Drug Loading of Eccentric Fe_3O_4@PAA/SiO_2 Core–Shell NCs. The drug storage of the eccentric Fe_3O_4@PAA/SiO_2 core–shell NCs as a drug carrier was monitored by UV–vis spectroscopy. Briefly, 126 μL of DOX aqueous solution (10 mg mL^{-1}) was mixed with 1 mL of eccentric Fe_3O_4@PAA/SiO_2 core–shell NCs (1 mg mL^{-1}) under stirring for 24 h. Then, the DOX-loaded eccentric Fe_3O_4@PAA/SiO_2 core–shell NCs were collected by an external magnetic field, and the supernatant was used to calculate the amount of DOX loaded into eccentric Fe_3O_4@PAA/SiO_2 core–shell NCs via a UV–vis spectrophotometer at 480 nm. The contents of DOX were measured to evaluate the DOX-loading efficiency. The loading efficiency (LE %) of DOX is calculated by using eq 1:

$$\text{LE}\ (\%) = [m_{(\text{total DOX})} - m_{(\text{DOX in supernatant})}]/m_{(\text{total DOX})} \times 100\% \quad (1)$$

DOX Release Behaviors of DOX-Loaded Eccentric Fe_3O_4@PAA/SiO_2 NPs. A semipermeable dialysis bag diffusion technique was used to measure the release of DOX from DOX-loaded eccentric Fe_3O_4@PAA/SiO_2 core–shell NCs. One mL of DOX-loaded eccentric Fe_3O_4@PAA/SiO_2 core–shell NCs was divided into two parts equally; then, the two parts were redispersed in 0.5 mL phosphate-buffer saline (PBS) solutions of pH 5.1 and pH 7.4, respectively. Subsequently, both of them were transferred into semipermeable dialysis bags, and the two bags were immersed into 3 mL of the corresponding PBS solution at 37 °C with gentle shaking. The DOX released from DOX-loaded eccentric Fe_3O_4@PAA/SiO_2 core–shell NCs could move out of the bags into PBS solution and was measured by a fluorescence spectrophotometer at an excitation and emission wavelength of 479 and 591 nm, respectively.

Cell Culture. Prostate cancer PC3M cells were maintained in a humidified incubator in Dulbecco's modified eagle medium (DMEM) containing 10% fetal bovine serum and cultured at 37 °C in an atmosphere of 95% air/5% CO_2.

Cell Uptake. To attach PC3M cells onto glass coverslips, 1×10^5 cells were seeded into a 24-well plate and cultured in DMEM supplemented with 10% fetal bovine serum under an atmosphere of 95% air/5% CO_2. Then, 1 μg mL^{-1} of DOX-loaded eccentric Fe_3O_4@PAA/SiO_2 core–shell NCs was added to the PC3M cells and incubated for 24 h. After being washed several times with PBS solution to remove the remaining NCs and dead cells, 300 μL of Hoechst 33342 (10 mg mL^{-1}) was added into the cells to stain the nuclei for 15 min. Finally, the cells were washed with PBS to remove excess dye molecules and then observed on a CLSM.

In Vitro Cytotoxicity against PC3M Cells. Standard 3-(4,5-dimethylthialzol-2-yl)-2,5-diphe-nyltetrazo-lium bromide (MTT) assays were used to evaluate cell cytotoxicity. PC3M cells were seeded into a 96-well plate at a density of 2.5×10^4 (100 μL) per well and incubated in the same conditions of cell uptake. Then, serial concentrations of empty eccentric Fe_3O_4@PAA/SiO_2 core–shell NCs, DOX-loaded eccentric Fe_3O_4@PAA/SiO_2 core–shell NCs, and free DOX in serum-free medium with 100 μL were mixed with the cells and incubated for 24 h. One row of a 96-well plate was only added in 100 μL of culture medium used as a control. Then, 20 μL of MTT solution (5 mg mL^{-1}) was added into each well with further incubation. The number of live cells can be calculated according to the amount of dark-blue formazan crystals that were produced by live cells. Afterward, dimethyl sulphoxide (DMSO) (150 μL) replaced the medium, and the absorbance (Abs) was measured at a wavelength of 490 nm on a microplate reader. Cell viability was counted by eq 2:

$$\text{cell viability}\ (\%) = \text{Abs}_{(\text{test cells})}/\text{Abs}_{(\text{reference cells})} \times 100\% \quad (2)$$

RESULTS AND DISCUSSION

The synthetic procedure for the synthesis of eccentric Fe_3O_4@PAA/SiO_2 core–shell NCs and application in pH-responsive controlled drug delivery and simultaneous cell imaging is shown in Scheme 1. In brief, OA-modified Fe_3O_4 NPs in chloroform were transferred to CTAB-modified Fe_3O_4 NPs in aqueous solution using CTAB as the stabilizing surfactant. After

successively adding PAA, ammonia solution, and isopropyl alcohol, the PAA molecules self-assembled around Fe_3O_4 NPs to obtain eccentric Fe_3O_4@PAA core−shell NPs. During this process, the resulting eccentric PAA shell is like a "reservoir" to absorb and retain water molecules inside its net structure because the PAA is a high water-absorbent polymer. It is well-known that TEOS has the remarkable property of easily converting into SiO_2 in the presence of water. Subsequently, TEOS and FITC conjugated with 3-APTMS were added into the solution, and the hydrolysis reaction of TEOS was confined to take place in the PAA network via taking advantage of the presence of water inside PAA shell. Therefore, the PAA can work as a template and nanoreactor for the SiO_2 condensation surrounding a single Fe_3O_4 NP to form fluorescent SiO_2 NCs that were composed of a large amount of small fluorescent SiO_2 NPs, resulting in the formation of FITC-labeled eccentric Fe_3O_4@PAA/SiO_2 core−shell NCs. Furthermore, the obtained NCs can perform as a drug vehicle with ultrahigh drug storage capacity and fluorescent label for simultaneous pH-responsive controlled drug delivery and cancer cell imaging in vitro.

Figure 1A,B shows the TEM images of OA and CTAB modified Fe_3O_4 NPs with an average diameter of about 25 nm, respectively. It can be seen that the CTAB modified Fe_3O_4 NPs are highly dispersed with no aggregations after being transferred into water phase (Figure 1B). To further coat the PAA shell onto the CTAB modified Fe_3O_4 NPs, excess CTAB molecules were removed by centrifuging three times in water. Subsequently, PAA aqueous solution, ammonia solution, and isopropyl alcohol were added to make the ratio of water/isopropyl alcohol to be 1:24; then, a PAA shell was successfully assembled on each Fe_3O_4 NP to obtain about 60 nm eccentric Fe_3O_4@PAA core−shell NPs, as shown in Figure 1C, which is attributed to the change of the interfacial energy of the synthetic system.[48,51−53] The inset in Figure 1C shows one part of a magnified TEM image of eccentric PAA shell. As PAA is an anionic polymer, carboxylic acid groups on the PAA chains are dissociated into carboxylate anions in a water solution at neutral pH, which can form hydrogen bonding with water molecules. This makes PAA capable of absorbing and retaining the water in organic phase as an excellent water-absorbent. That is, PAA shell encapsulating a Fe_3O_4 NP is like a "reservoir" to absorb and retain water molecules inside its net structure. Interestingly, upon the addition of TEOS, the formation of SiO_2 NPs was confined by the water molecules inside the PAA networks, and then, a large amount of small SiO_2 NPs was produced, constituting a SiO_2 NC with aggregated pores. Finally, the eccentric Fe_3O_4@PAA/SiO_2 core−shell NCs are achieved, as shown in Figure 1D, which are distinguished from other conventional concentric Fe_3O_4 coated with mSiO_2 materials.[32,33,35,54−56] As can be seen from Figure 1D, the as-prepared monodisperse NCs are uniform with an average size of about 100 nm and no free SiO_2 NPs appear. The inset in Figure 1D shows one part of a magnified TEM image of SiO_2 NCs. The SEM image confirms that the surface of Fe_3O_4@PAA/SiO_2 core−shell NCs is relatively rough, exhibiting SiO_2 NCs are composed of a large amount of small SiO_2 NPs, forming the aggregated mesopores (Figure 1E). The energy dispersive X-ray (EDX) spectrum obtained from Figure 1E shows the elements of the obtained Fe_3O_4@PAA/SiO_2 core−shell NCs (Figure 1F).

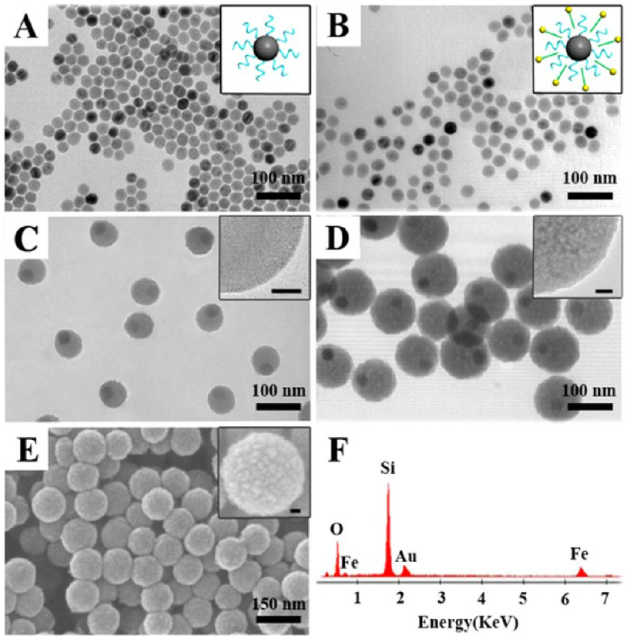

Figure 1. TEM images of (A) OA-modified Fe_3O_4 NPs, (B) CTAB-modified Fe_3O_4 NPs, (C) eccentric Fe_3O_4@PAA core−shell NPs, and (D) eccentric Fe_3O_4@PAA/SiO2 core−shell NCs; (E) SEM image of eccentric Fe_3O_4@PAA/SiO_2 core−shell NCs; (F) energy dispersive X-ray spectrum of eccentric Fe_3O_4@PAA/SiO_2 core−shell NCs. Insets in (C), (D), and (E) are magnified TEM and SEM images of the corresponding samples, respectively. Scale bars: 10 nm.

Moreover, the size of the NCs can be precisely controlled by varying the amount of TEOS during the formation of the SiO_2 NCs. Multifunctional eccentric Fe_3O_4@PAA/SiO_2 core−shell NCs with different diameters of about 80, 100, and 130 nm were fabricated (Figure 2A−C), respectively. The as-synthesized eccentric Fe_3O_4@PAA/SiO_2 core−shell NCs have relatively narrow size distributions that are consistent with TEM images (insets of Figure 2). The more TEOS added, the smaller were the SiO_2 NPs formed in the PAA network shell, leading to a bigger SiO_2 NC. The growth process of SiO_2 NCs with different sizes was accompanied with the swelling of PAA networks during the formation of small SiO_2 NPs inside the PAA shell.

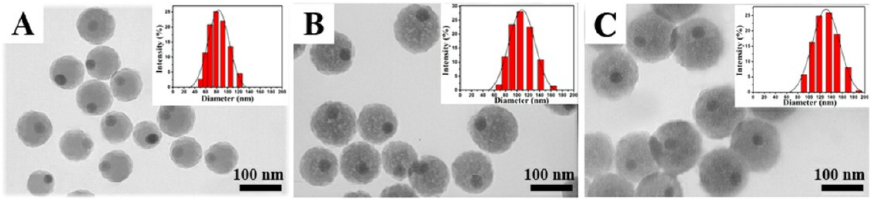

Figure 2. TEM images and size distributions (inset) of (A−C) about 80, 100, and 130 nm eccentric Fe_3O_4@PAA/SiO_2 core−shell NCs with different SiO_2 thicknesses.

dx.doi.org/10.1021/am401627u | ACS Appl. Mater. Interfaces 2013, 5, 7282−7290

To further confirm this simple synthetic process to be universal, it can be applied to other NPs with different compositions and shapes. For example, eccentric $NaYF_4$:Yb/Er/Gd@PAA/SiO_2 core–shell NCs using average diameters of about 20 nm and lengths of about 100 nm $NaYF_4$:Yb/Er/Gd NRs as cores were successfully synthesized. Figure 3A,B shows

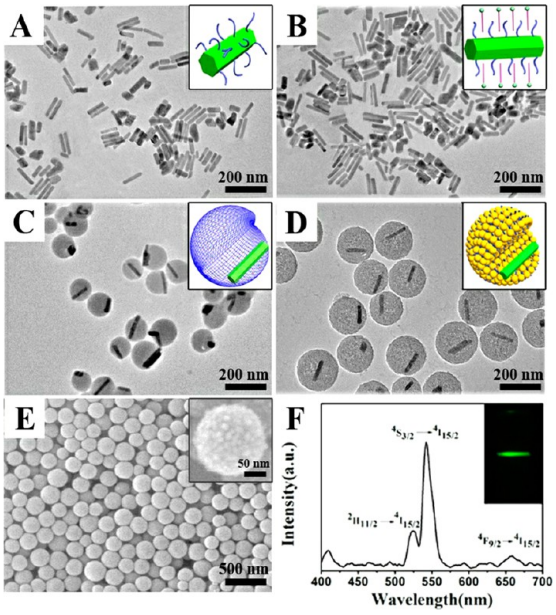

Figure 3. TEM images of (A) OA-modified $NaYF_4$:Yb/Er/Gd NRs, (B) CTAB-modified $NaYF_4$:Yb/Er/Gd NRs, (C) eccentric $NaYF_4$:Yb/Er/Gd@PAA core–shell NPs, and (D) eccentric $NaYF_4$:Yb/Er/Gd@PAA/SiO_2 core–shell NCs; (E) SEM image of eccentric $NaYF_4$:Yb/Er/Gd@PAA/SiO_2 core–shell NCs. The inset in (E) is a magnified SEM image. (F) Up-conversion fluorescence spectrum of NCs. The inset in (F) is digital picture of NCs excited with 980 nm in the dark.

monodisperse OA and CTAB capped $NaYF_4$:Yb/Er/Gd NRs, respectively, which were fabricated in the light of the previous method.[49] The synthetic process for the eccentric $NaYF_4$:Yb/Er/Gd@PAA and $NaYF_4$:Yb/Er/Gd@PAA/SiO_2 core–shell NCs was operated in the same way as in the case of the Fe_3O_4 NPs, as shown in Figure 3C,D. Furthermore, the SEM image of the eccentric $NaYF_4$:Yb/Er/Gd@PAA/SiO_2 core–shell NCs indicates that the SiO_2 NCs was also composed of small NPs (Figure 3E). Figure 3F shows the up-conversion emission spectra of NCs excited with a 980 nm diode laser with a power density of about 50 mW cm^{-2}, in which the emission bands at 521, 539, and 654 nm can be assigned to $2H_{11/2}$ $4I_{15/2}$, $4S_{3/2}$ $4I_{15/2}$, and $4F_{9/2}$ $4I_{15/2}$ of Er^{3+}, respectively. Besides, the obtained NCs excited with 980 nm in the dark appeared bright green color (inset of Figure 3F), demonstrating the NCs can be used as up-conversion cell imaging labels. These results further verify that our simple and highly repeatable synthetic process using PAA as a templating agent and nanoreactor can be a good scheme for the generalized fabrication of uniform various functional nanoparticle core@PAA/mSiO_2 core–shell NCs.

In this approach, it is worth noting that the PAA, a biodegradable superabsorbent and pH-responsive polymer, plays crucial roles as a nanoreactor and template in the formation of functional NP core @PAA/SiO_2 NCs and their applications in drug loading and delivery. First, PAA was utilized as superabsorbent polymer,[57,58] which is able to absorb and retain the water in the synthetic system for the hydrolysis reaction of TEOS. Second, PAA network was also employed as the template to support the SiO_2 NCs. Third, the negatively charged PAA networks bearing carboxylate anions on PAA chains encapsulated into NCs can bond positively charged anticancer drugs by the electrostatic attraction. Therefore, the as-fabricated functional NP core@PAA/SiO_2 NCs show potential applications in simultaneous bioimaging and pH-controlled drug delivery for cancer cells.

To illustrate the as-prepared NCs for the potential applications in nanomedicine, the fluorescent–magnetic eccentric Fe_3O_4@PAA/SiO_2 core–shell NCs (about 100 nm) were taken as an example to investigate their application in simultaneous fluorescence imaging and pH responsive drug delivery into cancer cells. The synthetic process for eccentric Fe_3O_4@PAA/SiO_2 core–shell NCs was monitored by FTIR spectroscopy (Figure 4). In Figure 4A, the peaks at 566 cm^{-1} that appear in three characteristic curves are assigned to the stretching modes of Fe–O, while CTAB results in the peak at 2921 cm^{-1} in curve a. The obvious peaks at 1712 cm^{-1} in curves b and c are attributed to the C=O stretching vibration in the carboxyl group, qualitatively indicating that the PAA polymer existed in Fe_3O_4@PAA core–shell NPs and Fe_3O_4@PAA/SiO_2 core–shell NCs. For eccentric Fe_3O_4@PAA/SiO_2 core–shell NCs, PAA networks were enwrapped in the SiO_2 NC shells. In curve c, the absorption at 1092 cm^{-1} results from Si–O–Si antisymmetric stretching vibrations, which implies the existence of a SiO_2 layer on the NP surface. Moreover, the amount of PAA in eccentric Fe_3O_4@PAA/SiO_2 core–shell NCs can be quantificationally determined by TG analysis (Figure 4B). The obvious weight loss is estimated to be about 48.6% by subtracting the weight loss of physical water, which is equal to

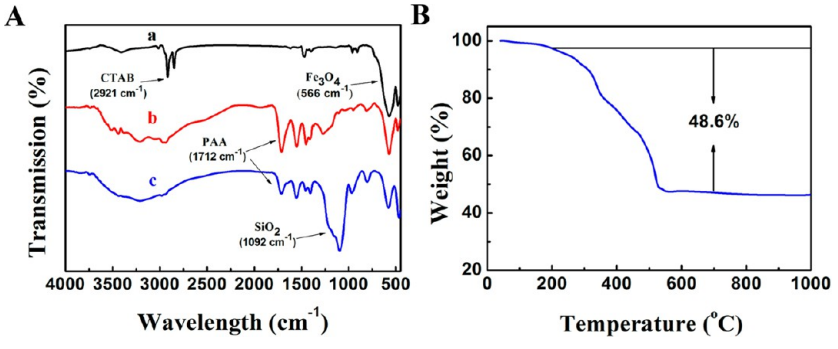

Figure 4. (A) FTIR spectra of (a) CTAB-modified Fe_3O_4 NPs, (b) eccentric Fe_3O_4@PAA core–shell NPs, and (c) eccentric Fe_3O_4@PAA/SiO_2 core–shell NCs. (B) TG curve of the eccentric Fe_3O_4@PAA/SiO_2 core–shell NCs.

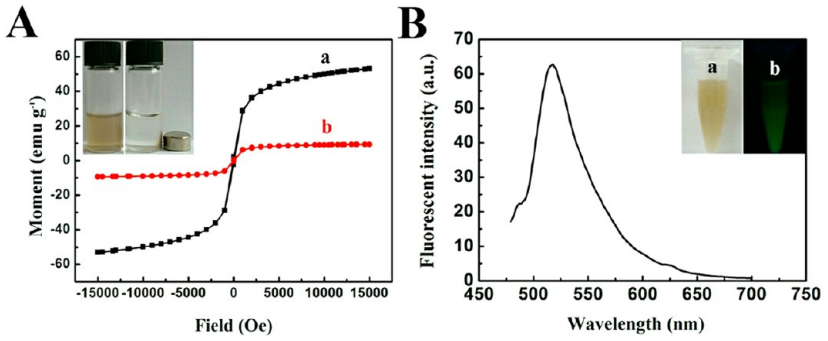

Figure 5. (A) Hysteresis loop measurements of (a) Fe_3O_4 NPs and (b) eccentric Fe_3O_4@PAA/SiO_2 core−shell NCs measured at 300 K, respectively. Insets: photographs of eccentric Fe_3O_4@PAA/SiO_2 core−shell NC solution without (left) and under (right) an external magnetic field. (B) Fluorescence spectrum of FITC-labeled eccentric Fe_3O_4@PAA/SiO_2 core−shell NCs (λ_{ex} = 458 nm). Inset: dispersion of FITC-labeled eccentric Fe_3O_4@PAA/SiO_2 core−shell NCs in water under (a) white light and (b) UV light.

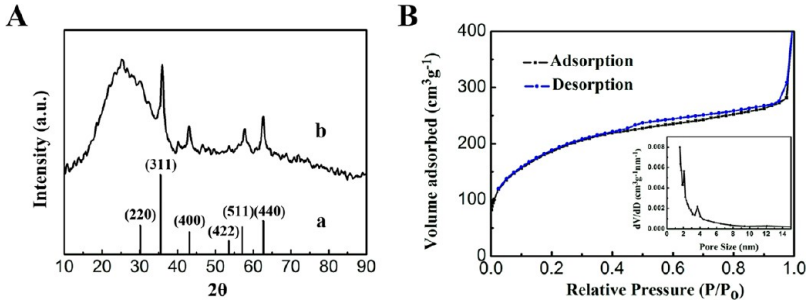

Figure 6. (A) XRD pattern of (a) Fe_3O_4 NPs, JCPDS 88-0315; (b) eccentric Fe_3O_4@PAA/SiO_2 core−shell NCs. (B) N_2 adsorption/desorption isotherm and pore size distribution curve (inset) of eccentric Fe_3O_4@PAA/SiO_2 core−shell NCs.

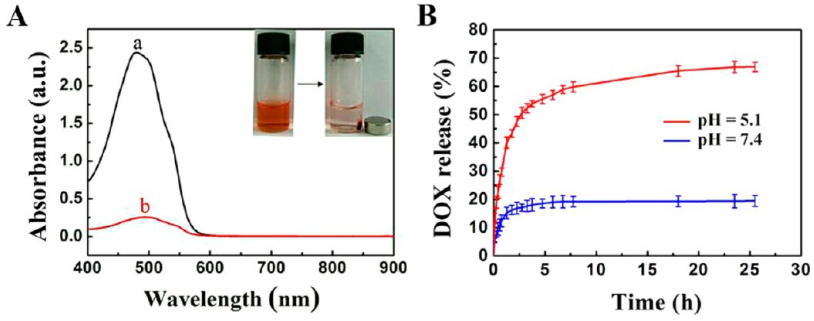

Figure 7. (A) UV−vis absorption spectra of DOX solutions before (a) and after (b) interacting with eccentric Fe_3O_4@PAA/SiO_2 core−shell NCs. Inset: photograph of eccentric Fe_3O_4@PAA/SiO_2 core−shell NCs just mixing with DOX aqueous solution (left) and after loading DOX for 24 h with an external magnet for magnetic separation (right). (B) DOX-release profiles for DOX-loaded Fe_3O_4@PAA/SiO_2 core−shell NCs measured in PBS buffer at pH 5.1 and 7.4 at 37 °C.

the amount of PAA in eccentric Fe_3O_4@PAA/SiO_2 core−shell NCs. These results confirm that the PAA polymer has successfully assembled onto CTAB modified Fe_3O_4 NPs and encapsulated in eccentric Fe_3O_4@PAA/SiO_2 core−shell NCs.

To investigate the magnetic properties of the samples, the as-prepared Fe_3O_4 NPs and eccentric Fe_3O_4@PAA/SiO_2 core−shell NCs were studied using a SQUID magnetometer at a temperature of 300 K (Figure 5A). The saturation magnetization value of eccentric Fe_3O_4@PAA/SiO_2 core−shell NCs is 9.35 emu g^{-1}, which is evidently lower than that of Fe_3O_4 (53.1 emu g^{-1}) due to the presence of the nonmagnetic PAA and SiO_2. However, the eccentric Fe_3O_4@PAA/SiO_2 core−shell NCs can be easily collected by an external magnet after being dispersed in aqueous solution (inset of Figure 5A). The result reveals that the as-synthesized eccentric Fe_3O_4@PAA/SiO_2 core−shell NCs exhibit good magnetic responsibility, suggesting their potential applications for magnetically targeted drug delivery, magnetic resonance imaging, and separation under an external magnetic field. To endow eccentric Fe_3O_4@PAA/SiO_2 core−shell NCs with multifunctionalities in the bioimaging and biolabeling applications, FITC conjugated with 3-APTMS was incorporated covalently into the SiO_2 shell using the co-condensation method. The obtained FITC-labeled eccentric Fe_3O_4@PAA/SiO_2 core−shell NCs show a typical emission of fluorescence at 517 nm, as shown in Figure 5B. As we know, if fluorescent dyes contact the Fe_3O_4 NPs, most of the fluorescence is quenched.[8,18,35] However, the obtained FITC-labeled eccentric Fe_3O_4@PAA/SiO_2 core−shell NCs emitted bright green color under UV light excitation (inset of Figure 5B). Therefore, the FITC-labeled eccentric Fe_3O_4@PAA/SiO_2 core−shell NC is a better candidate as a fluorescence label for bioimaging.

Figure 6A shows the XRD pattern of eccentric Fe_3O_4@PAA/SiO_2 core−shell NCs, of which all the diffraction peaks conform to that of standard Fe_3O_4 powers (JCPDS 880315). Besides, the peak around 25° is the characteristic peak of amorphous SiO_2. To study the specific surface area and porous nature of eccentric Fe_3O_4@PAA/SiO_2 core−shell NCs, N_2 adsorption/desorption measurements were performed. Figure 6B shows N_2 adsorption−desorption isotherm and pore size distribution of the as-fabricated NCs. The isotherm exhibits the type IV isotherm characteristics, and the corresponding Barrett−Joyner−Halenda (BJH) pore size distribution calculated using the adsorption/desorption isotherm branch (inset of Figure 6B) reveals that NCs have 2 and 3.7 nm mesopores, which allow drug molecules to pass through the shell. The mesoporous structures are possibly attributed to the aggregated small SiO_2 NPs, as shown in SEM images (Figure 1E). The Brunauer−Emmett−Teller (BET) surface area and the total pore volume were 674.9 $m^2\ g^{-1}$ and 0.325 $cm^3\ g^{-1}$. The result shows that the as-obtained eccentric Fe_3O_4@PAA/SiO_2 core−shell NCs with mesoporous structures and high surface area may possess high anticancer drug loading capacity as drug delivery carriers.

To explore the capability of the eccentric Fe_3O_4@PAA/SiO_2 core−shell NCs as anticancer drug delivery vehicles, DOX, a widely used typical anticancer drug, was chosen as a model drug. In pH 7.0 aqueous solution, DOX is positively charged, while carboxylic acid groups on the PAA chains are dissociated to carboxylate anions. Therefore, loaded DOX can form ionic bonds with the carriers by the robust electrostatic attraction. UV−vis spectroscopy was employed to measure the amount of DOX loaded into the NCs. Figure 7A shows the UV−vis absorption spectra of DOX aqueous solution before and after interacting with eccentric Fe_3O_4@PAA/SiO_2 core−shell NCs. DOX molecules are successfully loaded into the NCs, and it can be assumed through the obvious decrease of the absorption intensity of remaining DOX in the solution after interacting with the NCs, which can be further testified by the color change of supernatant and the NCs under an external magnetic field (inset of Figure 7A). The DOX loading efficiency is as high as 89.5%, and the drug loading amount is 1.13 mg per mg NCs, when 126 μL initial DOX solution (10 mg mL^{-1}) was added into 1 mg NCs. It is worth noting that the eccentric Fe_3O_4@PAA/SiO_2 core−shell NCs possess the much higher DOX loading compared with the previously reported mSiO_2-based NPs.[13,34,59−63] The result shows that the eccentric NCs are more favorable for loading a considerable amount of DOX as drug delivery carriers.

An efficient drug delivery system should not only have the capacity to store and transport drug molecules but also possess a sustained-release property. As a pH-responsive polymer, PAA can act as nanovalve for the release behaviors of DOX from DOX-loaded eccentric Fe_3O_4@PAA/SiO_2 core−shell NCs. Figure 7B shows the DOX release from DOX-loaded eccentric Fe_3O_4@PAA/SiO_2 core−shell NCs over a 24 h period in PBS with different pH values (5.1 and 7.4) at 37 °C, respectively. At pH 7.4, it can be seen that burst release occurs within 6 h to 19.4% and it remains unchanged even after 24 h, which will minimize the side effects to normal tissues. While at pH 5.1, a more acidic internal microenvironment in cancer cells, DOX can be released from the carrier due to the impairment of the electrostatic interaction of DOX with PAA as well as the enhancement of the solubility of DOX under acidic conditions, so 66.9% of the loaded DOX was released within 24 h. These results undoubtedly demonstrated that the Fe_3O_4@PAA/SiO_2 core−shell NCs drug delivery system have a strongly pH-dependent release of DOX. Furthermore, at different pH values, a sustained release profile is observed at the initial stage indicating that DOX-loaded eccentric Fe_3O_4@PAA/SiO_2 NCs have a sustained release property. As a result, eccentric Fe_3O_4@PAA/SiO_2 NCs could be used as drug delivery vehicles for cancer treatment.

Good cell uptake of carriers is an important characterization of an efficient drug-delivery system. CLSM is employed to evaluate the cell uptake of FITC-labeled eccentric Fe_3O_4@PAA/SiO_2 core−shell NCs. The CLSM images of PC3M cells incubated with DOX-loaded as-synthesized NCs are showed in Figure 8. Figure 8A is the CLSM image of nuclei (blue) of

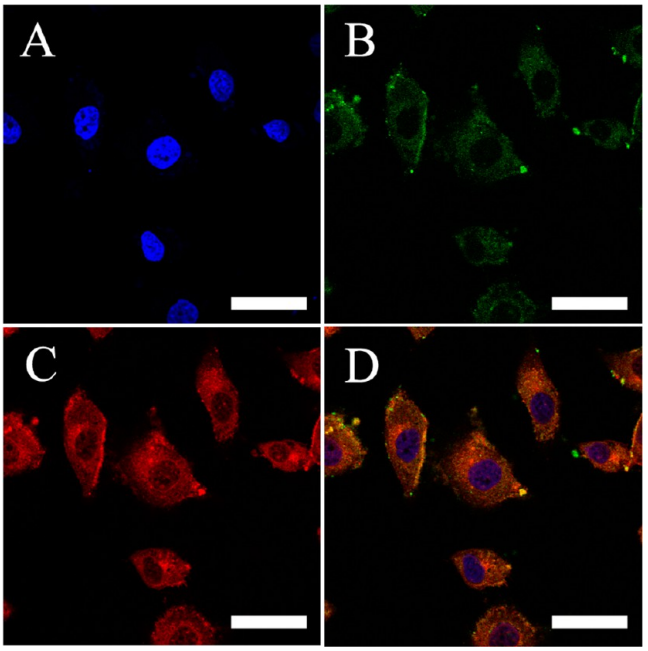

Figure 8. CLSM images of PC3M cells incubated with DOX-loaded FITC-labeled eccentric Fe_3O_4@PAA/SiO_2 core−shell NCs for 24 h. (A) The nuclei of cancer cells stained with blue Hoechest33342; (B, C) green fluorescence signals of FITC and red fluorescence signals of DOX of DOX-loaded FITC-labeled eccentric Fe_3O_4@PAA/SiO_2 core−shell NCs, respectively; (D) the merged image of (A−C). Scale bars: 50 μm.

cancer cells which was obtained after staining by Hoechst 33342. Figure 8B demonstrates considerable regions of the cytoplasm displaying strong green fluorescence, suggesting that the DOX-loaded FITC-labeled eccentric Fe_3O_4@PAA/SiO_2 core−shell NCs were efficiently localized within the cytoplasm. In this process, the DOX-loaded FITC-labeled eccentric Fe_3O_4@PAA/SiO_2 core−shell NCs enter into cancer cells via the endocytosis effect and form a vesicle at the cell membrane. Subsequently, the NCs enter into endosomes and lysosomes along with the vesicle and then move out of endosomes and lysosomes to release into the cytoplasm.[36,64] There are no green fluorescent signals of NPs in nuclei, suggesting that NCs do not locate into the cell nucleus. However, the red fluorescence signals of DOX appear in both the cytoplasm and the cell nucleus (Figure 8C), demonstrating that DOX was released from the eccentric NCs in the cytoplasm, subsequently entered into the nucleus of the PC3M cells. It is well-known that the DOX entering into tumor cells and accumulation in the

nucleus can enhance its antitumor activity. Figure 8D is the merged image of panels A–C. The results reveal the feasibility and efficiency of eccentric Fe_3O_4@PAA/SiO_2 core–shell NCs as drug delivery nanocarriers into cancer cells and fluorescence labels for simultaneous cell imaging.

Good drug vehicles in a drug delivery system should possess good biocompatibility, so the cytotoxicity of eccentric Fe_3O_4@PAA/SiO_2 core–shell NCs was investigated. The cytotoxic effects of the as-prepared NCs on PC3M cells were evaluated by MTT assays and are shown in Figure 9. Different

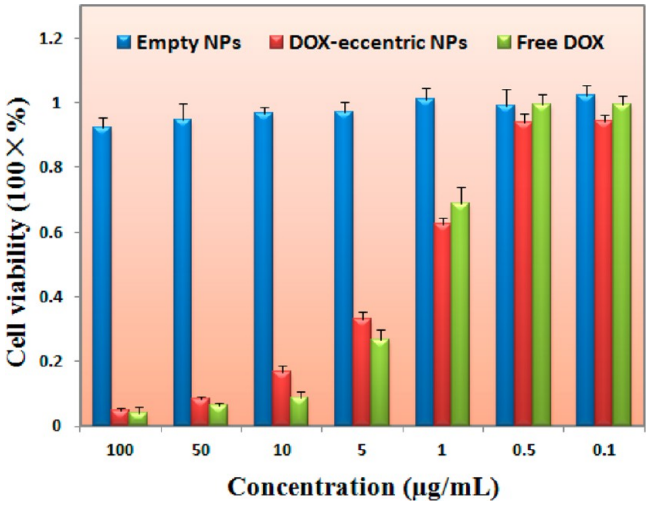

Figure 9. The cytotoxicity of empty eccentric Fe_3O_4@PAA/SiO_2 core–shell NCs, DOX-loaded eccentric Fe_3O_4@PAA/SiO_2 core–shell NCs, and free DOX against PC3M cells at different levels of concentration after 24 h, relatively.

concentration levels of empty eccentric Fe_3O_4@PAA/SiO_2 core–shell NCs, DOX-loaded NCs, and free DOX were incubated with prostate cancer PC3M cells for 24 h to evaluate cell viability. The result reveals that the cells maintained >90% cell viability after 24 h of treatment with the empty eccentric Fe_3O_4@PAA/SiO_2 core–shell NCs even at the concentration of 100 μg mL^{-1}, indicating that the NPs have low cytotoxicity to cells. The DOX-loaded Fe_3O_4@PAA/SiO_2 core–shell NCs show a similar cytotoxic effect with free DOX against PC3M cells under the same drug amounts used, which verifies that the released DOX from NCs is pharmacologically active. Therefore, the results suggest that eccentric Fe_3O_4@PAA/SiO_2 core–shell NCs are very efficient as a drug delivery vehicle.

CONCLUSIONS

In conclusion, we first develop a novel and facile method to fabricate a new and unique class of multifunctional eccentric Fe_3O_4@PAA/SiO_2 core–shell NCs consisting of a single Fe_3O_4 NP, PAA chains, and SiO_2 NCs that are composed of a large number of small fluorescent SiO_2 NPs using PAA as a nanoreactor and template. The fluorescence of FTIC-labeled eccentric SiO_2 NCs can effectively avoid quenching by Fe_3O_4 cores. Interestingly, the resulting eccentric PAA shell as a high water-absorbent polymer is like a "reservoir" to capture and retain water molecules inside its net structure to confine the growth of small SiO_2 NPs inside the PAA networks, resulting in the formation of an eccentric SiO_2 NC with aggregated pores. The thicknesses of uniform and well-dispersed SiO_2 NCs can also be precisely controlled by using different amounts of TEOS. Importantly, the synthetic method has been confirmed to be universal and extended to other functional NPs with different compositions and shapes as eccentric cores. Furthermore, the as-prepared multifunctional eccentric Fe_3O_4@PAA/SiO_2 core–shell NCs combining fluorescence imaging, high drug loading capacity, and pH-responsive drug release into one were taken as an example to study the applications in simultaneous fluorescence imaging and pH responsive drug delivery into prostate cancer PC3M cells. The results show that the DOX loading capacity can reach 113 wt %, much higher than the conventional mSiO_2 materials, and the release experiments identify a sustained-release behavior and a pH-dependent manner of DOX from the DOX-loaded eccentric Fe_3O_4@PAA/SiO_2 core–shell NCs. Moreover, the eccentric Fe_3O_4@PAA/SiO_2 core–shell NCs exhibit very low cytotoxicity against PC3M cells. Therefore, all these positive attributes allow this strategy to be used for developing multifunctional platforms based on different functional NPs as eccentric cores for various applications such as fluorescence imaging, MRI, and magnetically targeted drug delivery for cancer therapies and diagnostics.

AUTHOR INFORMATION

Corresponding Author

*E-mail: wangcg925@nenu.edu.cn (C.W.); wangtt@cust.edu.cn (T.W.).

Author Contributions

⊥L. Chen and L. Li contributed equally to this paper.

Notes

The authors declare no competing financial interest.

ACKNOWLEDGMENTS

We would like to thank the National Natural Science Foundation of China (Grant Nos. 21173038, 20703009), Natural Science Foundation and Science and Technology Development Planning of Jilin Province (201215003 and 201201115), and Science Foundation for Young Teachers of Changchun University of Science and Technology (XQNJJ-2011-11).

REFERENCES

(1) Selvan, S. T.; Patra, P. K.; Ang, C. Y.; Ying, J. Y. *Angew. Chem., Int. Ed.* **2007**, *46*, 2448–2452.
(2) Paula, A. J.; Stéfani, D.; Souza Filho, A. G.; Kim, Y. A.; Endo, M.; Alves, O. L. *Chem.—Eur. J.* **2011**, *17*, 3228–3237.
(3) Wu, H.; Liu, G.; Zhang, S.; Shi, J.; Zhang, L.; Chen, Y.; Chen, F.; Chen, H. *J. Mater. Chem.* **2011**, *21*, 3037–3045.
(4) Zhang, L.; Wang, T.; Li, L.; Wang, C.; Su, Z.; Li, J. *Chem. Commun.* **2012**, *48*, 8706–8708.
(5) Li, W.; Zhao, D. *Adv. Mater.* **2013**, *25*, 142–149.
(6) Liong, M.; Angelos, S.; Choi, E.; Patel, K.; Stoddart, J. F.; Zink, J. I. *J. Mater. Chem.* **2009**, *19*, 6251–6257.
(7) Angelos, S.; Johansson, E.; Stoddart, J. F.; Zink, J. I. *Adv. Funct. Mater.* **2007**, *17*, 2261–2271.
(8) Lai, C. W.; Wang, Y. H.; Lai, C. H.; Yang, M. J.; Chen, C. Y.; Chou, P. T.; Chan, C. S.; Chi, Y.; Chen, Y. C.; Hsiao, J. K. *Small* **2008**, *4*, 218–224.
(9) Liu, J.; Qiao, S. Z.; Hartono, B. S.; Lu, G. Q. *Angew. Chem., Int. Ed.* **2010**, *49*, 4981–4985.
(10) Liu, J.; Bu, W.; Zhang, S.; Chen, F.; Xing, H.; Pan, L.; Zhou, L.; Peng, W.; Shi, J. *Chem.—Eur. J.* **2012**, *18*, 2335–2341.
(11) Hou, Z.; Li, C.; Ma, P.; Li, G.; Cheng, Z.; Peng, C.; Yang, D.; Yang, P.; Lin, J. *Adv. Funct. Mater.* **2011**, *21*, 2356–2365.

(12) Yang, J.; Zhang, F.; Chen, Y.; Qian, S.; Hu, P.; Li, W.; Deng, Y.; Fang, Y.; Han, L.; Luqman, M.; Zhao, D. *Chem. Commun.* **2011**, *47*, 11618−11620.
(13) Zhang, Z.; Wang, L.; Wang, J.; Jiang, X.; Li, X.; Hu, Z.; Ji, Y.; Wu, X.; Chen, C. *Adv. Mater.* **2012**, *24*, 1418−1423.
(14) Yi, D. K.; Selvan, S. T.; Lee, S. S.; Papaefthymiou, G. C.; Kundaliya, D.; Ying, J. Y. *J. Am. Chem. Soc.* **2005**, *127*, 4990−4991.
(15) Song, Y.; Cao, X.; Guo, Y.; Chen, P.; Zhao, Q.; Shen, G. *Chem. Mater.* **2008**, *21*, 68−77.
(16) Santra, S.; Bagwe, R. P.; Dutta, D.; Stanley, J. T.; Walter, G. A.; Tan, W.; Moudgil, B. M.; Mericle, R. A. *Adv. Mater.* **2005**, *17*, 2165−2169.
(17) Liu, S.; Wong, Y.; Wang, Y.; Wang, D.; Han, M. Y. *Adv. Funct. Mater.* **2007**, *17*, 3147−3152.
(18) Liong, M.; Lu, J.; Kovochich, M.; Xia, T.; Ruehm, S. G.; Nel, A. E.; Tamanoi, F.; Zink, J. I. *ACS Nano* **2008**, *2*, 889−896.
(19) Qiao, R.; Yang, C.; Gao, M. *J. Mater. Chem.* **2009**, *19*, 6274−6293.
(20) Peng, J.; Feng, L. N.; Zhang, K.; Li, J. J.; Jiang, L. P.; Zhu, J. J. *Chem.—Eur. J.* **2011**, *17*, 10916−10923.
(21) Teng, Z.; Li, J.; Yan, F.; Zhao, R.; Yang, W. *J. Mater. Chem.* **2009**, *19*, 1811−1815.
(22) Park, H.; Yang, J.; Seo, S.; Kim, K.; Suh, J.; Kim, D.; Haam, S.; Yoo, K. H. *Small* **2008**, *4*, 192−196.
(23) Kim, J.; Lee, J. E.; Lee, S. H.; Yu, J. H.; Lee, J. H.; Park, T. G.; Hyeon, T. *Adv. Mater.* **2008**, *20*, 478−483.
(24) Park, K.; Lee, S.; Kang, E.; Kim, K.; Choi, K.; Kwon, I. C. *Adv. Funct. Mater.* **2009**, *19*, 1553−1566.
(25) Meng, H.; Liong, M.; Xia, T.; Li, Z.; Ji, Z.; Zink, J. I.; Nel, A. E. *ACS Nano* **2010**, *4*, 4539−4550.
(26) Lu, J.; Liong, M.; Li, Z.; Zink, J. I.; Tamanoi, F. *Small* **2010**, *6*, 1794−1805.
(27) Xia, T.; Kovochich, M.; Liong, M.; Meng, H.; Kabehie, S.; George, S.; Zink, J. I.; Nel, A. E. *ACS Nano* **2009**, *3*, 3273−3286.
(28) Wong, Y. J.; Zhu, L.; Teo, W. S.; Tan, Y. W.; Yang, Y.; Wang, C.; Chen, H. *J. Am. Chem. Soc.* **2011**, *133*, 11422−11425.
(29) Chen, T.; Chen, G.; Xing, S.; Wu, T.; Chen, H. *Chem. Mater.* **2010**, *22*, 3826−3828.
(30) Geng, J.; Li, M.; Chen, C.; Qu, X. *Adv. Healthcare Mater.* **2012**, *1*, 332−336.
(31) Chen, C.; Geng, J.; Pu, F.; Yang, X.; Ren, J.; Qu, X. *Angew. Chem., Int. Ed.* **2011**, *50*, 882−886.
(32) Ding, H. L.; Zhang, Y. X.; Wang, S.; Xu, J. M.; Xu, S. C.; Li, G. H. *Chem. Mater.* **2012**, *24*, 4572−4580.
(33) Lu, Y.; Yin, Y.; Mayers, B. T.; Xia, Y. *Nano Lett.* **2002**, *2*, 183−186.
(34) Zhu, Y.; Ikoma, T.; Hanagata, N.; Kaskel, S. *Small* **2010**, *6*, 471−478.
(35) Kim, J.; Kim, H. S.; Lee, N.; Kim, T.; Kim, H.; Yu, T.; Song, I. C.; Moon, W. K.; Hyeon, T. *Angew. Chem., Int. Ed.* **2008**, *47*, 8438−8441.
(36) Chen, Y.; Chen, H.; Ma, M.; Chen, F.; Guo, L.; Zhang, L.; Shi, J. *J. Mater. Chem.* **2011**, *21*, 5290−5298.
(37) Deng, Y.; Qi, D.; Deng, C.; Zhang, X.; Zhao, D. *J. Am. Chem. Soc.* **2007**, *130*, 28−29.
(38) Lu, A. H.; Salabas, E. L.; Schüth, F. *Angew. Chem., Int. Ed.* **2007**, *46*, 1222−1244.
(39) Lay, C. L.; Tan, H. R.; Lu, X.; Liu, Y. *Chem.—Eur. J.* **2011**, *17*, 2504−2509.
(40) Yang, X.; Chen, L.; Huang, B.; Bai, F.; Yang, X. *Polymer* **2009**, *50*, 3556−3563.
(41) Vallet-Regí, M.; Balas, F.; Arcos, D. *Angew. Chem., Int. Ed.* **2007**, *46*, 7548−7558.
(42) Yuan, L.; Tang, Q.; Yang, D.; Zhang, J. Z.; Zhang, F.; Hu, J. *J. Phys. Chem. C* **2011**, *115*, 9926−9932.
(43) Xing, L.; Zheng, H.; Cao, Y.; Che, S. *Adv. Mater.* **2012**, *24*, 6433−6437.
(44) Wen, H.; Guo, J.; Chang, B.; Yang, W. *Eur. J. Pharm. Biopharm.* **2013**, *84*, 91−98.
(45) Dai, Y.; Ma, P. A.; Cheng, Z.; Kang, X.; Zhang, X.; Hou, Z.; Li, C.; Yang, D.; Zhai, X.; Lin, J. *ACS Nano* **2012**, *6*, 3327−3338.
(46) Kang, X. J.; Dai, Y. L.; Ma, P. A.; Yang, D. M.; Li, C. X.; Hou, Z. Y.; Cheng, Z. Y.; Lin, J. *Chem.—Eur. J.* **2012**, *18*, 15676−15682.
(47) Ma, W. F.; Wu, K. Y.; Tang, J.; Li, D.; Wei, C.; Guo, J.; Wang, S. L.; Wang, C. C. *J. Mater. Chem.* **2012**, *22*, 15206−15214.
(48) Li, L.; Zhang, L.; Xing, S.; Wang, T.; Luo, S.; Zhang, X.; Liu, C.; Su, Z.; Wang, C. *Small* **2013**, *9*, 825−830.
(49) Lee, J. E.; Lee, N.; Kim, H.; Kim, J.; Choi, S. H.; Kim, J. H.; Kim, T.; Song, I. C.; Park, S. P.; Moon, W. K.; Hyeon, T. *J. Am. Chem. Soc.* **2009**, *132*, 552−557.
(50) Wang, F.; Han, Y.; Lim, C. S.; Lu, Y.; Wang, J.; Xu, J.; Chen, H.; Zhang, C.; Hong, M.; Liu, X. *Nature* **2010**, *463*, 1061−1065.
(51) Chen, T.; Yang, M.; Wang, X.; Tan, L. H.; Chen, H. *J. Am. Chem. Soc.* **2008**, *130*, 11858−11859.
(52) Xing, S.; Feng, Y.; Tay, Y. Y.; Chen, T.; Xu, J.; Pan, M.; He, J.; Hng, H. H.; Yan, Q.; Chen, H. *J. Am. Chem. Soc.* **2010**, *132*, 9537−9539.
(53) Feng, Y.; He, J.; Wang, H.; Tay, Y. Y.; Sun, H.; Zhu, L.; Chen, H. *J. Am. Chem. Soc.* **2012**, *134*, 2004−2007.
(54) Park, M.; Seo, S.; Lee, I. S.; Jung, J. H. *Chem. Commun.* **2010**, *46*, 4478−4480.
(55) Jeong, U.; Teng, X.; Wang, Y.; Yang, H.; Xia, Y. *Adv. Mater.* **2007**, *19*, 33−60.
(56) Tan, H.; Xue, J. M.; Shuter, B.; Li, X.; Wang, J. *Adv. Funct. Mater.* **2010**, *20*, 722−731.
(57) Lin, J.; Wu, J.; Yang, Z.; Pu, M. *Macromol. Rapid Commun.* **2001**, *22*, 422−424.
(58) Li, A.; Wang, A.; Chen, J. *J. Appl. Polym. Sci.* **2004**, *92*, 1596−1603.
(59) Chen, Y.; Chen, H.; Zhang, S.; Chen, F.; Zhang, L.; Zhang, J.; Zhu, M.; Wu, H.; Guo, L.; Feng, J.; Shi, J. *Adv. Funct. Mater.* **2011**, *21*, 270−278.
(60) Chen, Y.; Chen, H.; Guo, L.; He, Q.; Chen, F.; Zhou, J.; Feng, J.; Shi, J. *ACS Nano* **2009**, *4*, 529−539.
(61) Zhang, L.; Wang, T.; Yang, L.; Liu, C.; Wang, C.; Liu, H.; Wang, Y. A.; Su, Z. *Chem.—Eur. J.* **2012**, *18*, 12512−12521.
(62) Chen, F. H.; Zhang, L. M.; Chen, Q. T.; Zhang, Y.; Zhang, Z. J. *Chem. Commun.* **2010**, *46*, 8633−8635.
(63) Chen, Y.; Chen, H.; Zeng, D.; Tian, Y.; Chen, F.; Feng, J.; Shi, J. *ACS Nano* **2010**, *4*, 6001−6013.
(64) Tao, Z.; Toms, B.; Goodisman, J.; Asefa, T. *ACS Nano* **2010**, *4*, 789−794.